INVESTIGATION OF COMPOSITE ACTION IN BRIDGES BUILT WITH ADJACENT PRECAST INVERTED T-BEAMS AND CAST-IN-PLACE TOPPING

Fatmir Menkulasi, PE, Via Department of Civil and Environmental Engineering, Virginia Tech, Blacksburg, VA
Carin L. Roberts Wollmann, PhD, PE, Via Department of Civil and Environmental Engineering, Virginia Tech, Blacksburg, VA
Tommy Cousins, PhD, PE, Via Department of Civil and Environmental Engineering, Virginia Tech, Blacksburg, VA

ABSTRACT

Short to medium span composite bridges constructed with adjacent precast inverted T-beams and cast-in-place topping are intended to provide a higher degree of resiliency against reflective cracking and time dependent effects compared to voided slab and adjacent box girder systems. This paper investigates the composite action between the unique precast and cast-in-place element shapes. A full-scale composite beam has been tested under different loading arrangements with the purpose of simulating the service level design moment, strength level design shear, strength level design moment and nominal moment capacity. To investigate the necessity of extended stirrups one half of the span featured extended stirrups whereas the other half featured no extended stirrups. It is shown that the system behaved compositely at all loading levels and that no slip occurred at the interface. In addition to measuring slip at various interface locations full composite action has been verified by comparing load displacement curves obtained analytically and experimentally. It is concluded that because of the large contact surface between the precast and cast-in-place elements, cohesion alone appears to provide the necessary horizontal shear strength to ensure full composite action.

Keywords: Composite action, Cohesion, Extended stirrups

INTRODUCTION

Most bridge systems that consist of prefabricated elements and feature a jointless riding surface rely on some type of composite action. Typically, for concrete bridges, the term composite construction refers to the combination of precast girders with a cast-in-place deck or topping. The cast-in-place deck meets functional requirements by providing a smooth, useful surface and, in addition, substantially stiffens and strengthens the precast unit (Nilson[1]). When superimposed loads are applied to a composite system there is a tendency for the cast-in-place slab to slip horizontally, the bottom face of the slab tending to move outward with respect to the top face of the precast girder, which tends to displace inward (Nilson[1]). Preventing this slip is essential in ensuring full composite action and to do that there must be a means for transferring shear forces across the interface between the two components of the composite member. Resistance against interface shear forces can be provided by the natural adhesion and friction between the cast-in-place and precast components. Deliberately roughening the top surface of the precast girder enhances the contribution of adhesion and friction to the horizontal shear strength of the composite member. In addition, for composite systems that feature a broad interface, no other provisions need to be made to transfer the horizontal shear stresses. When the contribution of adhesion and friction are not sufficient, extended stirrups are typically provided to enhance slip resistance through dowel action and by holding the two components in intimate contact.

To ensure full composite action, the interface shear force must be smaller than the horizontal shear strength of the interface. There are various ways to calculate the interface shear force, or horizontal shear demand. When a beam is un-cracked and its behavior is linear elastic, horizontal shear stresses can be estimated using the following equation:

$$v_h = \frac{VQ}{Ib_v} \tag{1}$$

where:
V = vertical shear force at location under consideration
Q = first moment of area of portion above interface with respect to neutral axis
I = moment of inertia of composite cross-section
b_v = width of the interface

Loov[2] states that this equation can be used to evaluate the horizontal shear stress for cracked beams if Q and I are based on the cracked section. Because it provides a common basis for comparison, this equation was adopted in previous studies even though Hanson[3] and Saeman and Sasha[4] recognized that it does not give an exact representation of the horizontal shear stress at failure (Loov[2]). As an alternative to the classical elastic strength of materials approach, a reasonable approximation of the factored interface shear force at the strength or extreme event limit state for either elastic or inelastic behavior and cracked or uncracked sections can be provided by Equations 2 and 3[5].

$$V_{ui} = v_{ui} A_{cv} \quad (2)$$

where:

V_{ui} = factored interface shear force on area A_{cv} (kips)
v_{ui} = factored interface shear stress (ksi)
A_{cv} = area of concrete considered to be engaged in horizontal shear transfer (in.^{2})

$$v_{ui} = \frac{V_u}{b_{vi} d_v} \quad (3)$$

V_u = factored vertical shear force at section under consideration (kips)
b_{vi} = interface width considered to be engaged in shear transfer (in.)
d_v = the distance between the centroid of the tension steel and the mid-thickness of the slab to compute a factored interface shear stress (in.)

The interface shear force can also be calculated based on equilibrium conditions by computing the actual change in compressive or tensile force in any segment[6]. For example if the change in the compressive force over a segment of length l_v is C, and if the width of the interface is b_v, then the horizontal shear stress can be computed by Equation 4, which implies that the entire length of the shear span can be used to transfer the horizontal shear force:

$$v_{ui} = \frac{C}{b_v l_v} \quad (4)$$

where:

C = change in the compressive force over a segment of length l_v

Loov[2] explains how Equations 1, 3 and 4 are closely related although they appear different. For example in Equation 1 the term VQ/I represents the rate of change of force in the flange. Equation 4 represents the average rate of change of force in the flange in segment whose lengths is l_v. For beams subject to points loads, Equations 1 and 4 would yield the same result because the vertical shear diagram between the points loads will be constant. For beams subject to uniformly distributed loads Equation 4 misses the locations with the highest horizontal shear stress because it reports only the average shear stress in the segment under consideration. Also, Equation 3 is similar to Equation 4 because V= dM/dx is the rate of change of moment. Loov[2] states that if the compression block is entirely within the flange, and the small variation in the depth of the stress block is ignored, then the compression force C will be equal to M/(d-a/2) and the rate of change of force in the flange will be V/(d-a/2). Therefore V/d_v is simply a non-conservative simplification of Eq.1[2].

After the horizontal shear demand has been determined a method for estimating the horizontal shear capacity is required to design for composite action. According to AASHTO LRFD Specifications[5] the nominal shear resistance of the interface plane shall be taken as:

$$V_{ni} = cA_{cv} + \mu\left(A_{vf}f_y + P_c\right) \leq minimum \begin{cases} K_1 f_c' A_{cv} \\ K_2 A_{cv} \end{cases} \quad (5)$$

in which:

$A_{cv} = b_{vi}L_{vi}$

where:

A_{vf} = area of interface shear reinforcement crossing the shear plane within the area A_{cv} (in.^{2})
L_{vi} = interface length considered to be engaged in shear transfer (in.)
c = cohesion factor specified in Article 5.8.4.3 (ksi)
μ = friction factor specified in Article 5.8.4.3
f_y = yield stress of reinforcement but design value not to exceed 60 ksi.
P_c = permanent net compressive force normal to the shear plane; if force is tensile, P_c = 0.0 kip. (kips)
f'_c = specified 28-day compressive strength of the weaker concrete on either side of the interface (ksi)
K_1 = fraction of concrete strength available to resist interface shear, as specified in Article 5.8.4.3 of AASHTO LRFD Specifications[5]
K_2 = limiting interface shear resistance specified in Article 5.8.4.3 (ksi)

Equation 5 is a modified shear friction model accounting for a contribution, evident in the experimental data, from cohesion and/or aggregate interlock depending on the nature of the interface under consideration given by the first term[5]. This equation is similar to the one used to estimate the vertical shear capacity of a concrete section, $V_c + V_s$, where V_c represents the shear strength provided by concrete and V_s the shear strength provided by transverse reinforcing steel.

Article 5.8.4.4 of AASHTO LRFD Specifications[5] requires a minimum area of interface shear reinforcement, which can be estimated by Equation 6.

$$A_{vf} \geq \frac{0.05\,A_{cv}}{f_y} \quad (6)$$

Prior to 2006 AASHTO LRFD Specifications[7] and AASHTO Standard Specifications[8] have required a minimum area of reinforcement based on the full interface area; similar to Equation 6, irrespective of the need to mobilize the strength of the full interface area to resist the applied factored interface shear[5]. In 2006, additional minimum area provisions, applicable only to girder slab interfaces were introduced with the purpose of eliminating the need for additional interface shear reinforcement due simply to a beam with a wider top flange being utilized in place of a narrower flanged beam[5]. These additional provisions are provided below for convenience:

- The minimum interface shear reinforcement, A_{vf}, need not exceed the lesser of the amount determined using Equation 6 and the amount needed to resist $1.33V_{ui}/\phi$ as determined using Equation 2.
- The minimum reinforcement provisions specified herein shall be waived for girder/slab interfaces with surface roughened to an amplitude of 0.25 in. where the factored interface shear stress, v_{ui} of Equation 3, is less than 0.210 ksi, and all vertical (transverse) shear reinforcement required by the provisions of Article 5.8.1.1 is extended across the interface and adequately anchored in the slab.

The first bulleted item establishes a rational upper bound for the area of interface shear reinforcement required based on the interface shear demand rather than the interface area as stipulated by Equation 6[5]. This treatment is analogous to minimum reinforcement provisions for flexural capacity where a minimum additional overstrength factor of 1.33 is required beyond the factored demand[5]. The second bulleted item suggests that an intentionally roughened surface can be expected to achieve 210 psi of horizontal shear resistance, but still requires the vertical shear reinforcing to be extended into the slab.

The inverted T-beam system is a new bridge system that consists of adjacent precast inverted T-beams with tapered webs, covered with a cast-in-place topping. This bridge system is intended to provide a higher degree of resiliency against reflective cracking and time dependent effects compared to voided slab and adjacent box girder systems[9,10]. This system is being implemented for the first time in Virginia, on US 360, near Richmond. Figure 1(a) shows the elevation of the US 360 Bridge and Figure 1(b) shows the transverse cross-section of the bridge. US 360 Bridge is a two-span continuous bridge. The clear span for the precast inverted T-beams is approximately 41 feet. Because of the unique shape of the precast beam, the composite action behavior of this bridge system was of interest and was investigated by testing a full-scale typical composite cross-section to failure. The purpose of the research presented in this paper is to:

- Investigate whether full composite action can be maintained at service and strength level design loads as well as under loads that simulate the nominal moment capacity of the composite section,
- Investigate the necessity of extended stirrups to ensure full composite action and determine whether cohesion alone can provide the necessary horizontal shear strength to achieve full composite action,
- Investigate the applicability of cohesion and friction factors stipulated in AASHTO[5] and those recommended by other researchers to the uniquely shaped composite section described herein,
- Investigate the necessity of minimum horizontal shear reinforcing provisions stipulated in AASHTO[5] for the interface condition described herein

PREVIOUS STUDIES

French et al.[11] investigated composite action behavior in composite bridges built with adjacent precast inverted T-beams with straight webs and covered with a cast-in-place topping. This investigation was carried out by testing two laboratory bridge specimens named Concept 1 and Concept 2. Concept 1 laboratory bridge specimen consisted of two spans whereas Concept 2 laboratory bridge specimen consisted of a single span. The horizontal shear reinforcing used in Span 2 of the Concept 1 bridge was based on AASHTO LRFD Specifications[5], whereas Span 1 was constructed with fewer horizontal shear reinforcing bars and did not satisfy the minimum horizontal shear reinforcing requirements of 2005 AASHTO LRFD Specifications[5]. The Concept 2 laboratory bridge was constructed with no horizontal shear reinforcing. Both bridge specimens had a standard raked finish (1/4 in. rake) on the top horizontal surface of the precast web. Furthermore, each specimen had a roughened diamond pattern with approximately 1/8 in. to ¼ in. perturbations on the vertical web surfaces of the precast panels[11]. Likewise, East span of the Concept 1 bridge, which was constructed with the 5 ¼ in. thick precast flange, also had the tops of the precast flanges roughened with the same diamond pattern[11]. It should be noted that the inverted T-beam system investigated by French et al.[11] featured transverse hooked bars in the precast elements that protruded from the precast webs into the cast-in-place topping.

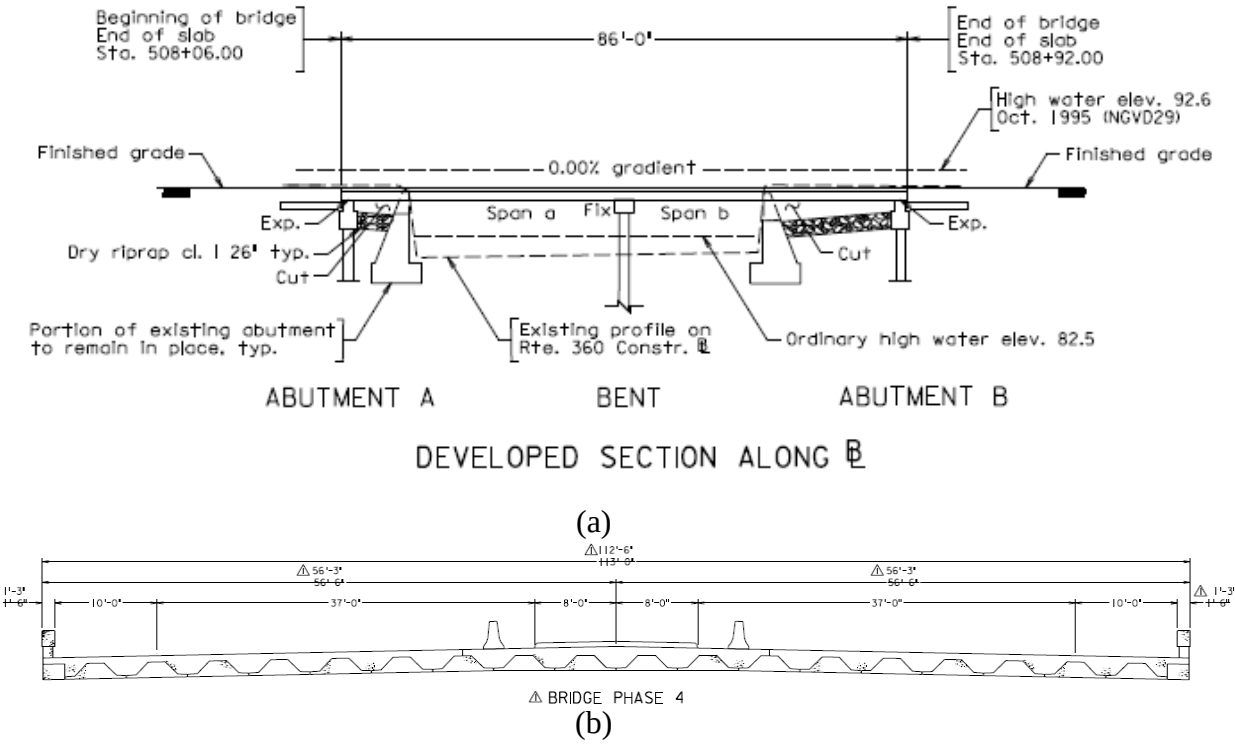

Figure 1. (a) Elevation of US 360 Bridge, (b) Transverse cross-section of US 360 Bridge

In the tests on both spans of Concept 1 laboratory bridge and on Concept 2 laboratory bridge, the sections were observed to remain composite well beyond service load levels, through the full range of loading to the maximum capacity of the loading system, which was in excess of the predicted nominal capacity of the Concept 1 and 2 bridges[11].

Longitudinal strains measured throughout the depth of the composite cross-sections indicated linear distributions, which evince full composite action. The Kent and Park[12] model was used to determine the corresponding compressive stress distribution in the CIP section assuming unconfined concrete models[11]. Tested values were used for the maximum compressive concrete strength and a corresponding concrete strain assumed to be 0.002 at the maximum compressive stress. Integrating the nonlinear stress distribution, resulted in an estimate of the maximum compression force achieved in the slab during loading to the ultimate capacity[11]. The horizontal shear stress estimated in the system at the precast-CIP interface was subsequently calculated by dividing the total compression force by half of the center-to-center of bearing span length and the total width of the bridge structure, and was determined to be 135 psi[11]. This method of calculating the horizontal shear stress is based on the approach presented by Equation 4 and gives an average horizontal shear stress. In addition, this method assumes that the failure mode in horizontal shear consists of a horizontal shear plane.

French et al.[11] concluded that AASHTO LRFD Specifications[5] should allow for the design of composite bridges with adjacent precast inverted T-beams with straight webs without horizontal shear ties, and allow the development of a maximum factored horizontal shear stress of 135 psi in sections with intentionally roughened surfaces (i.e., ¼ in. rake) unreinforced for horizontal shear. The proposed friction factor was based on AASHTO LRFD Specifications[5] for surfaces intentionally roughened to an amplitude of 0.25 in. The K_1 and K_2 values, which provide upper bound estimates of the horizontal shear capacity of a given section, selected to be used in the proposed specification modifications are simply the smallest, or most conservative of the existing K_1 and K_2 values[11]. The proposed specification recommendations by French et al.[11] are as follows (recommendations are in italics):

5.8.4.3 Cohesion and Friction Factors

The following values shall be taken for cohesion, c, and friction factor, μ:

…..

For concrete placed against a clean concrete surface, free of laitance, but not intentionally roughened:

c = 0.075 ksi
μ = 0.6 ksi
K_1 = 0.2
K_2 = 0.8 ksi

For normal weight concrete placed against a clean concrete surface, free of laitance, with surface intentionally roughened to an amplitude of 0.25 in. and no interface shear

reinforcement provided crossing the shear plane up to the minimum required A_{vf} in Eq. 5.8.4.4-1:

c = 0.135 ksi
μ = 1.0
K_1 = 0.2
K_2 = 0.8 ksi

5.8.4.4 Minimum Area of Interface Shear Reinforcement

……

- The minimum reinforcement provisions specified herein shall be waived for girder/slab interfaces with surface roughened to an amplitude of 0.25 in. where the factored interface shear stress, v_{ui} of Equation 3, is less than 0.210 ksi, and all vertical (transverse) shear reinforcement required by the provisions of Article 5.8.1.1 is extended across the interface and adequately anchored in the slab.
- *For the cast-in-place concrete of precast-composite slab-span systems that is cast on clean precast inverted-T surfaces free of laitance, with a surface intentionally roughened to an amplitude of ¼ in., the minimum reinforcement provisions specified herein shall be waived.*

C5.8.4.4

……

With respect to a girder/slab interface, the intent is that the portion of the reinforcement required to resist vertical shear which is extended into the slab also serves as interface shear reinforcement.

In the case of precast-composite slab-span systems, research (French et al. 2010) has shown that transverse reinforcement was not required across the CIP-precast interface in order to achieve composite action. Similar results were obtained in studies by Naito et al. (2008).

Because composite bridges constructed with the precast inverted T-beams with tapered webs and cast-in-place topping represent a unique composite cross-sectional shape, the applicability of existing provisions in AASHTO LRFD Design Specifications[5], and the recommendations proposed by French et al. was investigated.

EXPERIMENTAL INVESTIGATION

A full scale composite beam representing a typical transverse section was tested with the purpose of investigating its performance under design service level and strength level moments and shears. To investigate the necessity of extended stirrups half of the composite beam span featured extended stirrups whereas the other half did not. Initially, extended stirrups were provided along the entire span of the precast beam, however, prior to the placement of the cast-in-place topping half of them were cut off.

Figure 2 (a) shows the cross-sectional dimensions of the composite section. Figure 2 (b) shows the reinforcing details for half of the span that featured extended stirrups, whereas Figure 2 (c) features the reinforcing details for the other half. All precast surfaces in contact with the cast-in-place topping were roughened. The tapered precast webs and the tops of the precast flanges were roughened in the longitudinal direction to enhance composite action in the transverse direction of the bridge. Full composite action in the transverse direction is desired to avoid delamination at the precast beam cast-in-place topping interface because of transverse bending caused by wheel loads. Figure 3 illustrates the roughened precast surfaces.. The roughened surface on the tapered webs was created by using steel forms, the inside of which featured the pattern shown in Figure 4. The top of the precast flanges was roughened in the longitudinal direction by using a traditional ¼ in. rake finish. The top of the precast web was roughened in the transverse direction by performing a ¼ in. rake finish to enhance composite action in the longitudinal direction.

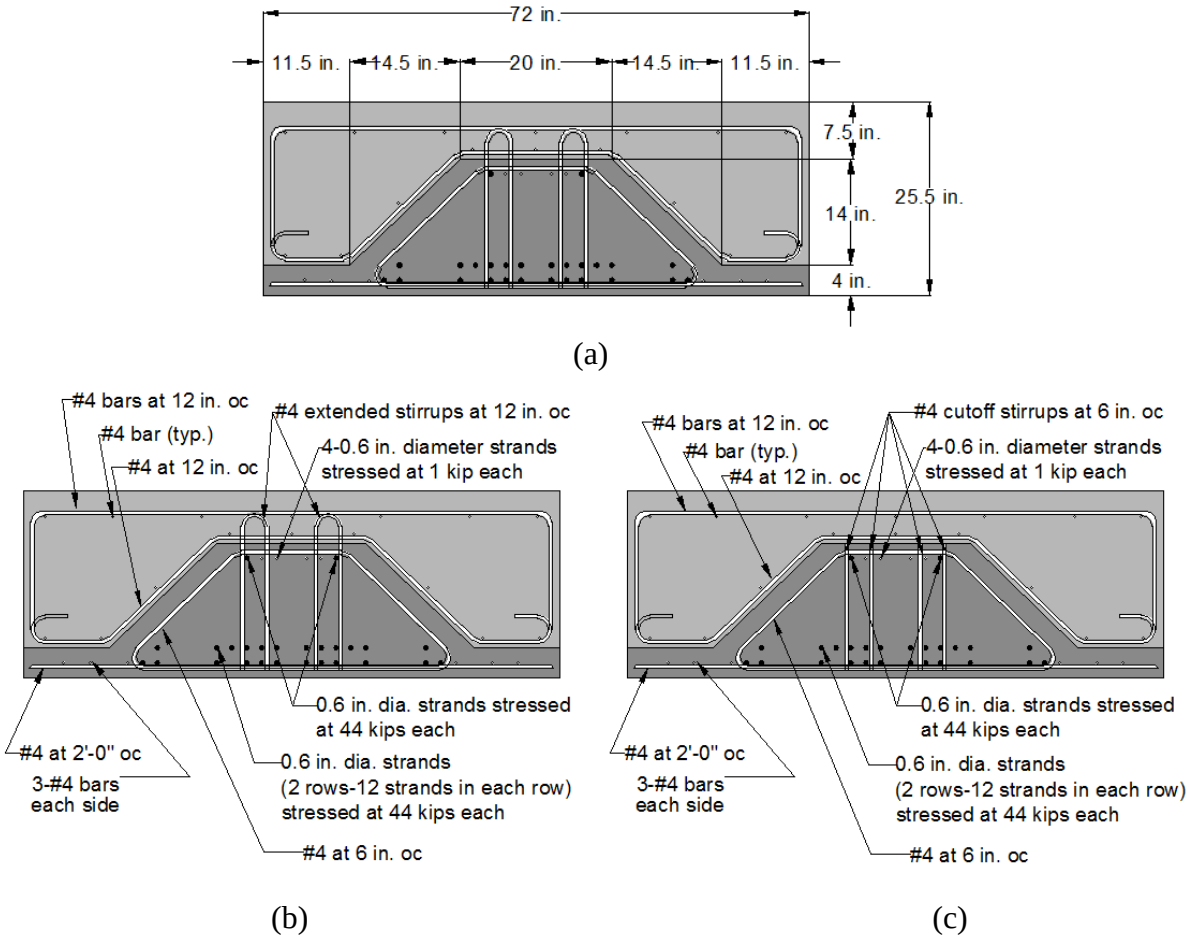

Figure 2. (a) Composite beam cross-section, (b) half of the span with extended stirrups, (c) the other half of the span without extended stirrups.

Figure 5 shows the elevation of the composite beam and some of the instrumentation used to verify composite action. A displacement sensor (denoted WP-7) was used at mid-

span with the purpose of comparing the load versus mid-span deflection curve obtained experimentally with that obtained analytically assuming full composite action. Displacements sensors were also used at quarter points (denoted WP-8 and WP-6) with the purpose of comparing the load versus quarter span deflection curves, provided that half of the span contained extended stirrups whereas the other half had no extended stirrups. Identical load versus quarter span deflections curves serve as evidence that the presence of extended stirrups is not required to enhance composite action.

Figure 3. Roughened precast surfaces

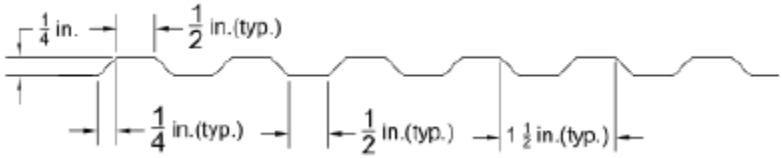

Figure 4. Roughened surface pattern in the longitudinal direction

A photograph of the test setup is provided in Figure 6 featuring the loading frame near mid-span. A 220 kip closed-loop servo controlled hydraulic actuator powered by a 30 gallons per minute hydraulic pump was used to load the composite system monotonically. A pin support was provided at one end of the beam and a roller support was provided at the other end to accommodate any potential longitudinal translation during testing. The pin support was provided by a solid circular steel section which rested on an assembly of a semicircular steel pipe section and a channel welded together to receive the solid steel section and create an assembly that allowed rotation but not longitudinal translation. Similarly, the roller support was provided by welding individual quarter circle steel pipe sections to a steel channel to create an assembly that allowed rotation and longitudinal translation at the same time (Figure 5 and Figure 7). The precast flanges at the ends of the precast beam were terminated one foot short from the end of the beam to prevent high flexural stresses in the precast flanges at the bearing points (such as abutments and intermediate supports). The cast-

in-place topping for the tested full scale beam followed the outline of the precast beam at the ends.

In addition to the displacement sensors, ten linear variable differential transformers (LVDT's) were used to ensure that there was no slip during the various loading stages. Loss of composite action would be manifested as a relative slip between the precast and the cast-in-place components. Five LVDT's were used at each end (Figure 7) to capture any potential slip. The LVDT's at each end consisted of one installed at the interface between the top of the precast web and the cast-in-place topping, two installed at the interface between the precast flanges and the cast-in-place topping and two others installed near the ends of the composite beam but on the sides, at the interface between the precast flanges and the cast-in-place topping.

Table 1 provides a summary of the moments and shears that each individual precast inverted T-beam in the US 360 Bridge was expected to be subject to. The moments and shears due to each load case are tabulated, and that information was used to calculate design moments and shears using Service I and Strength I load combinations. Three tests were performed with the purpose of simulating the maximum service level positive moment, the maximum strength level shear, the maximum strength level positive moment and the nominal moment capacity of the composite section. During the first test the simply supported beam was subject to two point loads symmetrical about mid-span (Figure 8 (a)). The two point loading was applied by attaching a spreader beam to the actuator and by supporting the spreader beam on two tire prints 4 ft. apart. The 4 ft. spacing was intended to represent tandem axle spacing. The actuator load required to simulate the maximum service level positive moment was estimated to be 40 kips (20 kips on each tire print). During this test the composite beam was expected to remain un-cracked and behave elastically.

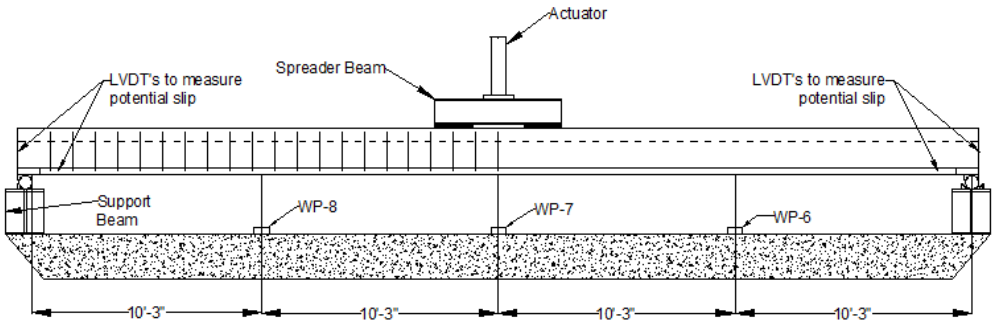

Figure 5. Drawing of Test Setup

Figure 6. Photograph of Test Setup

Figure 7. Location of LVDT's at the ends of the composite beam to measure slip.

Table 1. Design moments and shear for each composite beam at service and at ultimate.

Service (Service I)			
Moments (ft-kips)		**Shears (kips)**	
$+M_{invT}$	173	V_{invT}	17
$+M_{deck}$	231	V_{deck}	22
$+M_{live}$	297	V_{live}	45
$-M_{live}$	219		
$+M_{superD}$	60	V_{superD}	12
$-M_{superD}$	107		
$+M_{service}$ = 761			
Ultimate (Strength I)			
$+M_u$	**1100**	$V_{ucritical}$	138
$-M_u$	516		

The purpose of the second test was to simulate the strength level design shear. The loading frame was moved from mid-span to the position described in Figure 8 (b). The actuator load required to simulate strength level design shear was estimated to be 118 kips (59 kips on each tire print). The strength level design vertical shear was simulated on the portion of the composite beam without any extended stirrups with the purpose of subjecting the most critical half of the span to the design vertical shear force. The underlying logic in this approach was that if the half of the span without any extended stirrups could resist the design vertical shear force without incurring any slip, then the other half should be able to at least offer a comparable performance. Even though the actuator load in this test simulated strength level design shear forces, the behavior of the composite beam was expected to be linear elastic when tested material properties were considered.

During the third and the final test, the loading frame was moved back to the mid-span of the composite beam and the load was increased monotonically to simulate strength level design positive moment and the nominal positive moment capacity (Figure 8 (c)).

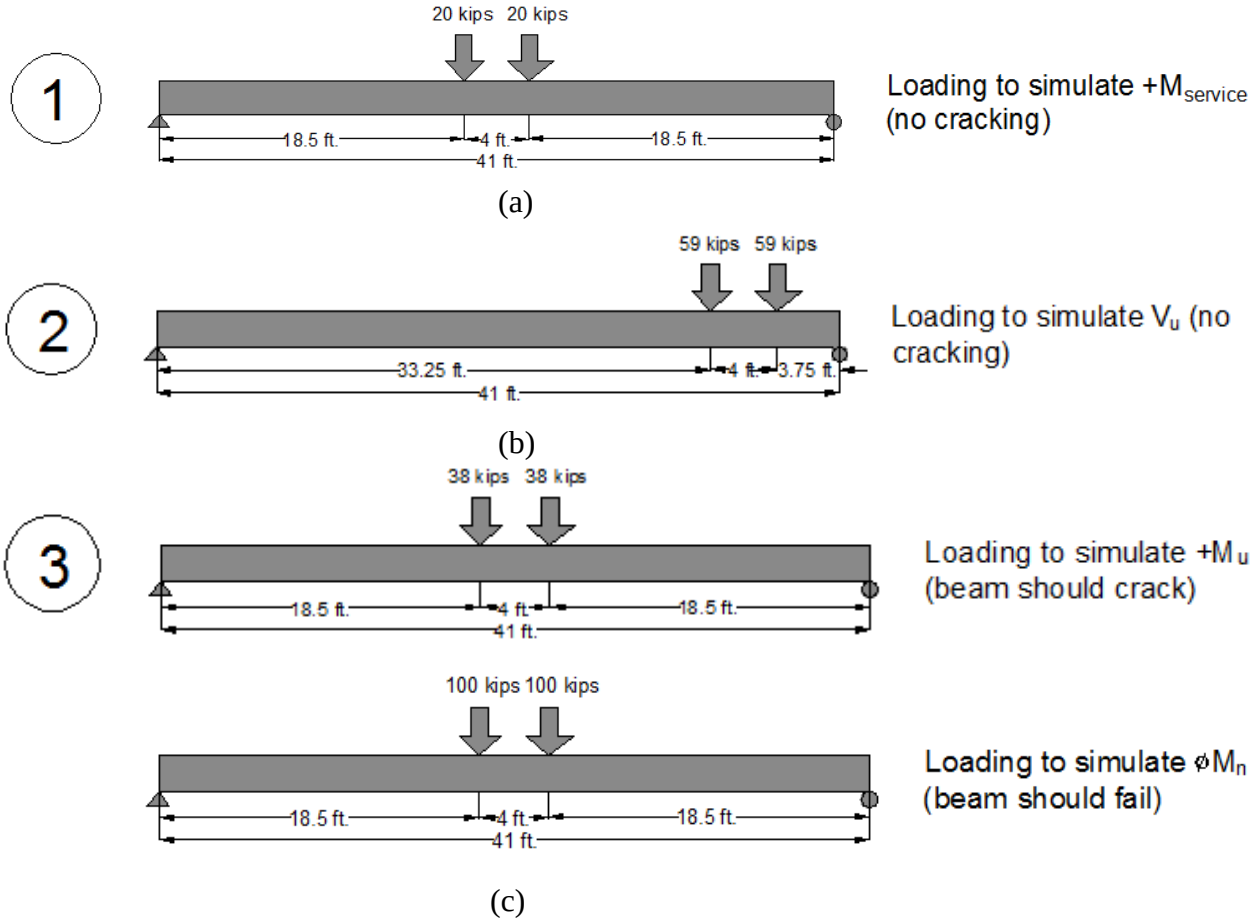

Figure 8. Summary of loading arrangements for the three tests, (a) simulation of service level design positive moment, (b) simulation of strength level design vertical shear, (c) simulation of strength level design positive moment and nominal moment capacity

ANALYTICAL INVESTIGATION

Before the three tests were conducted, an estimation of the vertical and horizontal shear capacity of the composite beam was performed based on AASHTO LRFD Design Specifications[5] using several assumptions. These estimations were conducted to ensure that the composite beam had adequate vertical and horizontal shear strength to resist the loads induced during the three tests. In addition, an estimation of the actuator load versus mid-span deflection curve was conducted , assuming full composite action, with the purpose of comparing this curve with the one obtained experimentally.

ESTIMATION OF VERTICAL SHEAR CAPACITY

The estimation of the vertical shear capacity was performed in accordance with Article 5.8.3.3 of AASHTO LRFD Design Specifications[5] based on Equations 7, 8 and 9. In addition, the vertical shear strength provided by concrete was calculated using the entire composite cross-section and the lower concrete compressive strength (f'_c = 4 ksi). Furthermore, this estimation was conservatively based on the simplified procedure for non-prestressed sections. Vertical stirrups were considered to provide shear strength only if they are extended in the cast-in-place topping. The presence of the bent transverse bars in the cast-in-place topping and the closed stirrups that encompass the prestressing strands in the precast beam were considered to contribute towards the vertical shear resistance of the composite section. Vertical shear demand was calculated at the critical section and was based on the loads simulated during Test 2. This information is provided in Table 2. The last column in Table 2 gives the ratio of the vertical shear demand to the vertical shear capacity. It can be observed that even when the contribution of the extended stirrups is ignored the demand to capacity ratio is still considerably lower than one.

$$V_n = min \begin{cases} V_c + V_s + V_p \\ 0.25\, f_c' b_v\, d_v + V_p \end{cases} \quad (7)$$

$$V_c = 0.0316\beta\sqrt{f_c'}\, b_v\, d_v \quad (8)$$

$$V_s = \frac{A_v f_y\, d_v\, (\cot\theta + \cot\alpha)\sin\alpha}{s} \quad (9)$$

Table 2 Calculated vertical shear demand and vertical shear strength

	Vertical Shear Strength (kips)					Vertical Shear Demand	Ratio
	ϕV_c	ϕV_s			$\phi V_n = \phi V_c + \phi V_s$	V_u (kips)	$V_u / \phi V_n$
		$\phi V_{sextended}$	$\phi V_{sinclinedPC}$	$\phi V_{sbentCIP}$			
Portion ***without*** extended stirrups	168	0	82	62	312	138	0.44
Portion ***with*** extended stirrups	168	82	82	62	394	138	0.35

ESTIMATION OF HORIZONTAL SHEAR CAPACITY

To determine whether slip could be prevented a comparison of the horizontal shear demand and capacity was performed. Horizontal shear demand was based on the loads simulated during Test 2 and was determined using Equations 1, 3 and 4 (Table 3). Because the composite beam remained un-cracked during Test 2 the utilization of Equation 1 using transformed un-cracked section properties was appropriate. Equation 1 yields higher horizontal shear stresses in Plane 1 compared to Plane 2 because Plane 1 is closer to the neutral axis, which is where horizontal shear stresses are highest in an un-cracked section. A single horizontal shear stress

value for Plane 3 could not be calculated using Equation 1 because Plane 3 consists of sub-planes whose distances to the neutral axis vary. Equation 3, yielded a similar horizontal shear stress value with that calculated for Plane 1 using Equation 1, which confirms that it provides a reasonable approximation of the horizontal shear stress. An examination of the derivation of Equation 3 reveals that this equations does not differentiate between horizontal shear stresses in any horizontal plane between the internal compression and tension forces. Also, because Equation 3 is a reasonable approximation for calculating horizontal shear stresses in horizontal planes, it does not apply to Plane 3. For the loading arrangement illustrated in Test 2, Equation 4 yields the average horizontal shear stress between the point of maximum moment to the point of zero moment. Because the shear diagram between these two points is not constant the horizontal shear stress calculated using Equation 4 is lower than that calculated using either Equation 1 or 3, which capture the maximum horizontal shear stress or an approximation of it.

Horizontal shear capacity was calculated based on AASHTO LRFD Specifications[5] (Equation 10). In the estimation of the horizontal shear capacity, three potential slip planes were considered (Figure 9). Plane 1 consists of the interface between the top of the precast web and the cast-in-place topping plus the rest of the width of the composite section. Plane 1 includes an intentionally roughened interface in the transverse direction and monolithic planes. Plane 2 consists of the interfaces between the precast flanges and cast-in-place topping and the bottom width of the precast beam web. Plane 2 includes intentionally roughened interfaces in the longitudinal direction and a monolithic plane. Plane 3 consists of the entire interface between the precast and cast-in-place components and includes roughened interfaces in the transverse and longitudinal directions. The horizontal shear capacity for each plane was calculated by using the appropriate cohesion and friction factors for the type of interfaces that each plane consisted of. The cohesion and friction factors for the assumed interface conditions are provided in Table 4.

Table 3. Horizontal shear stress (Test 2 – Simulation of strength level design shear)

Equation	**Horizontal shear stress (psi)**		
	Plane 1	Plane 2	Plane 3
1	99	65	Varies
3	96	96	NA
4	46	46	40

NA = not applicable

$$V_{ni} = cA_{cv} + \mu\left(A_{vf}f_y + P_c\right) \leq min \begin{cases} K_1 f_c' A_{cv} \\ K_2 A_{cv} \end{cases} \quad (10)$$

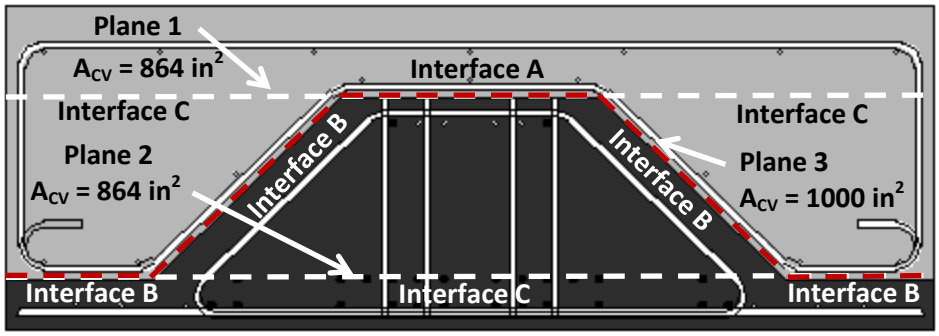

Figure 9. Potential failure planes due to horizontal shear

Table 4. AASHTO LRFD Specification[5] cohesion and friction factors

	Interface A (Intentionally roughened)	Interface B (Not intentionally roughened)	Interface C (monolithic)
Cohesion (c)	0.28	0.075	0.40
Friction (μ)	1	0.6	1.4
K_1	0.3	0.2	0.25
K_2	1.8	0.8	1.5

In addition, the estimation of the horizontal shear capacity was performed by both accounting for the presence of the extended stirrups and ignoring them. The results of this estimation are provided in Table 5. The horizontal shear demand and capacity values provided in Table 5 were calculated for one foot of length. The horizontal shear demand in terms of force was calculated by multiplying the horizontal shear stress values in Table 3 by the corresponding interface areas. The last six columns shows the ratio between the horizontal shear demand and capacity and suggest that a horizontal shear failure should not occur. As stated earlier, one of the goals of this study was to investigate experimentally whether adequate horizontal shear strength in such a uniquely shaped composite member can be provided solely by the natural cohesion between the two components.

Table 5. Comparison of estimated design horizontal shear force and horizontal shear capacity

	Demand (kips) (per foot of length)			**Capacity (kips) (per foot of length)**						**Ratio**					
Eq.	Plane 1	Plane 2	Plane 3	Plane 1		Plane 2		Plane 3		Plane 1		Plane 2		Plane 3	
				St.	No St.	St.	No St.	St.	No st.	St.	No St.	St.	No St.	St.	No st.
1	86	56	Varies	493	317	368	256	204	124	0.17	0.27	0.15	0.22	Varies	
3	83	83	NA	493	317	368	256	204	124	0.17	0.26	0.23	0.32	NA	
4	46	46	40	493	317	368	256	204	124	0.09	0.15	0.13	0.18	0.2	0.32

St. = with stirrups, No St. = without stirrups, NA=not applicable

ESTIMATION OF FULL LOAD VERSUS MID-SPAN DISPLACEMENT CURVE

To verify full composite action behavior of the system under various stages of loading, the full anticipated load versus mid-span deflection curve of the simply supported beam system

was estimated analytically for comparison with the load versus mid-span deflection curve obtained experimentally. To do this, material models defining the stress strain relationships for the two types of concrete and the prestressing steel present in the composite system had to be adopted.

Stress-strain relationship

For the precast and CIP concrete materials the Hognestad model was adopted and calibrated to match the tested compressive strength at 28 days. The design compressive strengths for the precast and cast-in-place components were f'_c = 6 ksi and f'_c = 4 ksi, respectively. The tested compressive strengths for the precast and cast-in-place components were 10.2 ksi and 8.5 ksi, respectively. The model consists of a second degree parabola with apex at a strain ε_0, which is the strain when f_c reaches f'_c. In this case ε_0 was taken equal to 0.0025. This model is described mathematically in Eq.11 and graphically in Figure 10. The maximum usable concrete strain was taken equal to 0.004. This model is convenient for use in analytical studies involving concrete because the entire stress-strain curve is given by one continuous function. The material model for the prestressing steel consisted of a tri-linear curve, which is mathematically described by the piecewise functions in Eq.12 and illustrated in Figure 11.

$$f_c = f'_c\left[\frac{2\varepsilon_c}{\varepsilon_0} - (\frac{\varepsilon_c}{\varepsilon_0})^2\right] \tag{11}$$

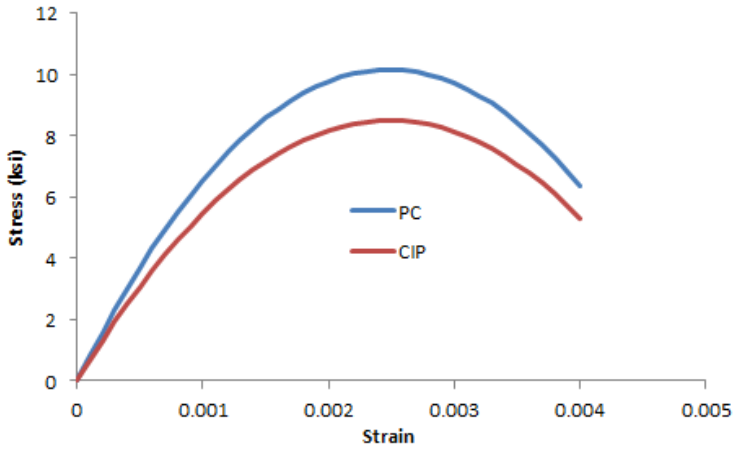

Figure 10. Stress strain relationship for concrete

$$f_{ps} = \begin{cases} f_{ps} = E_{ps}\,\varepsilon_{ps} & \text{if } \varepsilon_{ps} \le 0.0084 \\ f_{ps} = 240 + 1515(\varepsilon_{ps} - 0.0084) & \text{if } 0.0084 \le \varepsilon_{ps} \le 0.015 \\ f_{ps} = 250 + 444(\varepsilon_{ps} - 0.015) & \text{otherwise} \end{cases} \tag{12}$$

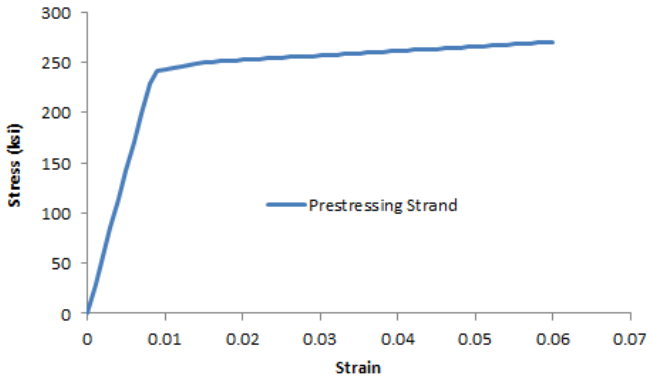

Figure 11. Stress strain relationship for prestressing strand

Moment Curvature Relationship

To obtain the anticipated full load versus mid-span deflection curve for the simply supported composite beam a moment curvature relationship had to be developed for any given cross-section of the beam. Because the system consists of a pre-tensioned precast beam with straight strands and a cast-in-place topping the moment-curvature relationship was constant throughout the span. After the moment curvature relationship is defined, this information can be used to relate the moment diagram in the simply supported beam to a curvature diagram, which can then be used to calculate deflections at desired locations along the span.

Up to first crack

The moment curvature relationship up until the first crack was calculated using principles from linear elastic mechanics of materials. For the non-composite section strain profiles along the depth of the section were obtained by first calculating the stresses at the extreme fibers (Eq. 13) and then dividing them by the modulus of elasticity of the precast beam (Eq.14). Curvatures were calculated based on the slope of the strain diagram (Eq.15) and moments were calculated using statics (Eq. 16). For the composite section additional moments and curvatures up to first crack were calculated by using the section properties of the composite section (Eq. 18-20). The cracking moment due to actuator load was calculated by assuming a modulus of rupture equal to $7.5\sqrt{f'c}$ (Eq. 17). Total curvatures in the composite system up until the first crack were calculated simply by adding the additional curvatures due to loads in the composite system to the already calculated ones on the precast beam. Total moments were calculated using statics.

The slope of the moment curvature curve defines the flexural stiffness of the precast before it was made composite and that of the composite system after the cast-in-place topping was placed. The difference in these slopes is illustrated in Figure 14 (a).

Non-composite section

$$\sigma = \mp\frac{P_e}{A_{pc}} \mp \frac{P_e e\, y}{I_{pc}} \mp \frac{(M_{invT} + M_{cip})12\, y}{I_{pc}} \quad (13)$$

$$\varepsilon = \frac{\sigma}{E} \quad (14)$$

$$\emptyset_{noncomposite} = \frac{\varepsilon_{bottom} - \varepsilon_{top}}{h_{pc}} \quad (15)$$

$$M_{noncomposite} = M_{invT} + M_{cip} \quad (16)$$

Composite section

$$M_{cracking} = \frac{\frac{1}{12}\left[f_r + \frac{P_e}{A_{pc}} + \frac{P_e e\, y_{botcomp}}{I_{pc}} - \frac{(M_{invT} + M_{cip})12\, y_{botcomp}}{I_{pc}}\right] I_c}{y_{botcomp}} \quad (17)$$

$$\Delta\varepsilon = \mp\frac{M_{cracking}\, 12\, y}{I_c E_{pc}} \quad (18)$$

$$\Delta\emptyset = \frac{\Delta\varepsilon_{bot} - \Delta\varepsilon_{top}}{h_{pc}} \quad (19)$$

$$M_{composite} = M_{noncomposite} + M_{cracking} \quad (20)$$

$$\emptyset = \emptyset_{noncomposite} + \Delta\emptyset \quad (21)$$

After cracking

An algorithm was used to obtain the moment curvature relationship in the composite section after cracking. This algorithm is described in Figure 12 and Figure 13 and consists of incrementally increasing the strain in the top of the cast-in-place concrete and finding the corresponding depth of the neutral axis. The strain in the top of the cast-in-place concrete and the depth to the neutral axis are used to calculate strain and stress profiles in the composite section. Compressive stress profiles in concrete are integrated to calculate internal compressive forces and the tensile stress in steel is used to calculate the internal tension force. After internal equilibrium is satisfied, the internal moment, curvatures and the depth to the neutral axis are reported. Nilson[1] states that the relatively small strain discontinuity at the interface between precast and cast-in-place concrete, resulting from prior bending of the non-composite precast section, can been ignored without serious error at the overload stage. Because the strain range covered in this algorithm is relatively large, the strain discontinuity at the interface was ignored. However, the discontinuity of the concrete stress profiles at the interface of the two components was taken into account for cases when the neutral axis falls below the thinnest portion of the cast-in-place concrete topping.

Because the data from the test will include the superimposed load (actuator load) versus the corresponding mid-span deflection the full moment curvature relationship (Figure 14 (a)) is adjusted to reflect just the superimposed moment and the corresponding curvature (Figure 14(b)). This information is then used to construct a curvature diagram based on the moment

diagram in the composite beam caused by the actuator load. Deflection at mid-span of the beam is then calculated by multiplying the individual areas in the curvature diagram by the distance between their centroids and the support (Eq.22).

$M\phi :=$ count $\leftarrow 1$

for $\varepsilon_{ciptop} \in 0.001, 0.0011 .. 0.004$

for $c_{depth} \in 0.01, 0.02 .. 13$

$\phi \leftarrow \frac{\varepsilon_{ciptop}}{c_{depth}}$

$\varepsilon_s \leftarrow \frac{\varepsilon_{ciptop}}{c_{depth}} \cdot (h - c_{depth} - y_{cgsb})$

$\varepsilon_{stotal} \leftarrow \varepsilon_{sp} + \varepsilon_{ce} + \varepsilon_s$

$\sigma_s \leftarrow E_{ps} \cdot \varepsilon_{stotal}$ if $\varepsilon_{stotal} \le 0.0084$

$\sigma_s \leftarrow 240 + 1515 \cdot (\varepsilon_{stotal} - 0.0084)$ if $0.0084 < \varepsilon_{stotal} \le 0.015$

$\sigma_s \leftarrow 250 + 444 \cdot (\varepsilon_{stotal} - 0.015)$ otherwise

$T \leftarrow \sigma_s \cdot A_{ps}$

if $c_{depth} > h_{cip}$

$C_{cip1} \leftarrow \int_{(c_{depth} - h_{cip})}^{c_{depth}} f_{cCIP} \left[\frac{2 \cdot \phi \cdot x}{\varepsilon_o} - \left(\frac{\phi \cdot x}{\varepsilon_o} \right)^2 \right] \cdot b_{cip} \, dx$

$b_{cip2} \leftarrow b_{cip} - b_{PCtop} - (c_{depth} - h_{cip}) \cdot 2$

$C_{cip2} \leftarrow \int_{0}^{(c_{depth} - h_{cip})} f_{cCIP} \left[\frac{2 \cdot \phi \cdot x}{\varepsilon_o} - \left(\frac{\phi \cdot x}{\varepsilon_o} \right)^2 \right] \cdot b_{cip2} \, dx$

$\sigma_{cip3} \leftarrow f_{cCIP} \left[\frac{2 \cdot \phi \cdot (c_{depth} - h_{cip})}{\varepsilon_o} - \left[\frac{\phi \cdot (c_{depth} - h_{cip})}{\varepsilon_o} \right]^2 \right]$

$C_{cip3} \leftarrow 2 \cdot \left[\frac{1}{3} \cdot (c_{depth} - h_{cip})^2 \cdot \frac{1}{2} \cdot \sigma_{cip3} \right]$

$C_{PC1} \leftarrow \int_{0}^{(c_{depth} - h_{cip})} f_{cpc} \left[\frac{2 \cdot \phi \cdot x}{\varepsilon_o} - \left(\frac{\phi \cdot x}{\varepsilon_o} \right)^2 \right] \cdot b_{PCtop} \, dx$

$\sigma_{PC2} \leftarrow f_{cpc} \left[\frac{2 \cdot \phi \cdot (c_{depth} - h_{cip})}{\varepsilon_o} - \left[\frac{\phi \cdot (c_{depth} - h_{cip})}{\varepsilon_o} \right]^2 \right]$

$C_{PC2} \leftarrow 2 \cdot \left[\frac{1}{3} \cdot (c_{depth} - h_{cip})^2 \cdot \frac{1}{2} \cdot \sigma_{PC2} \right]$

$C_{total} \leftarrow C_{cip1} + C_{cip2} + C_{cip3} + C_{PC1} + C_{PC2}$

Continues on Figure 13

Figure 12. Partial algorithm for calculating Moment Curvature Relationship

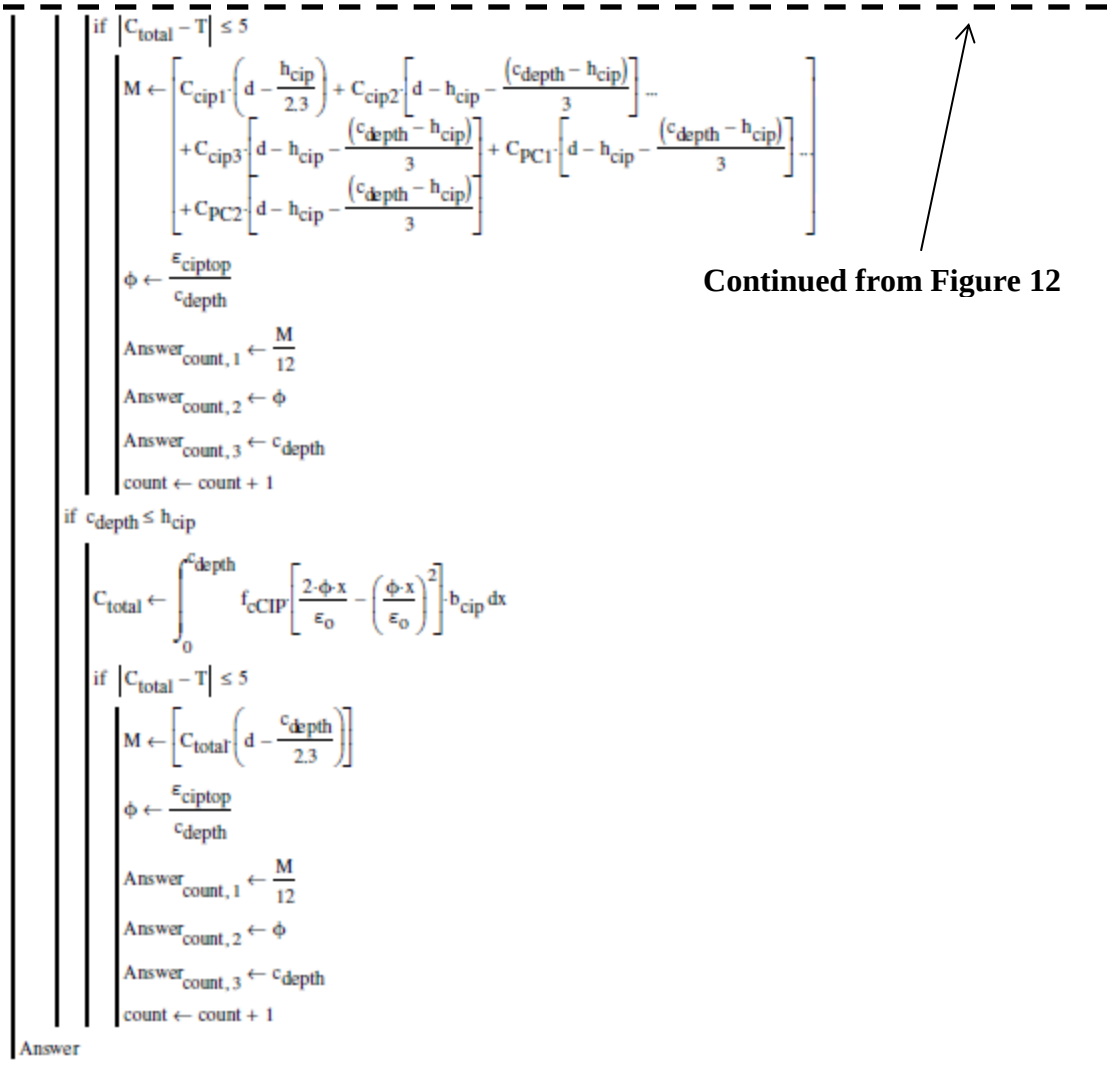

Figure 13. Partial algorithm for calculating Moment Curvature Relationship

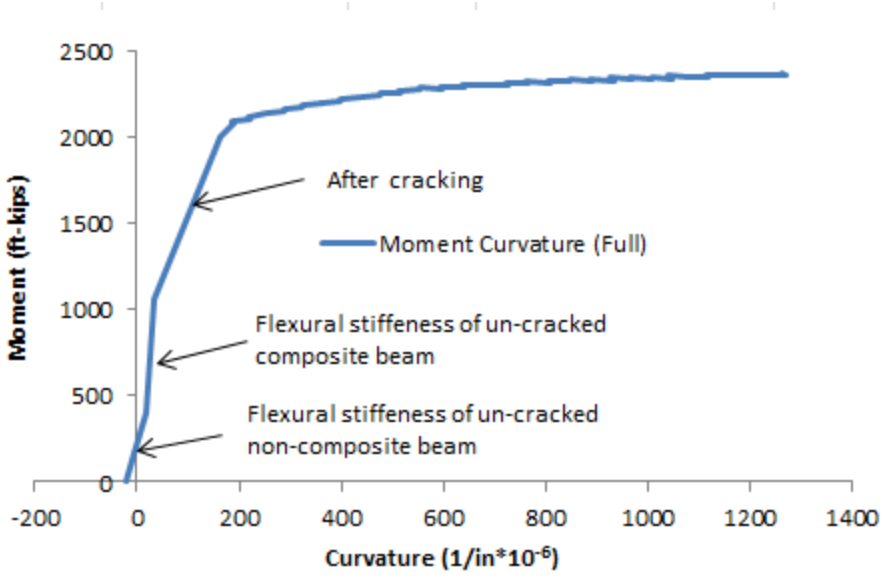

(a)

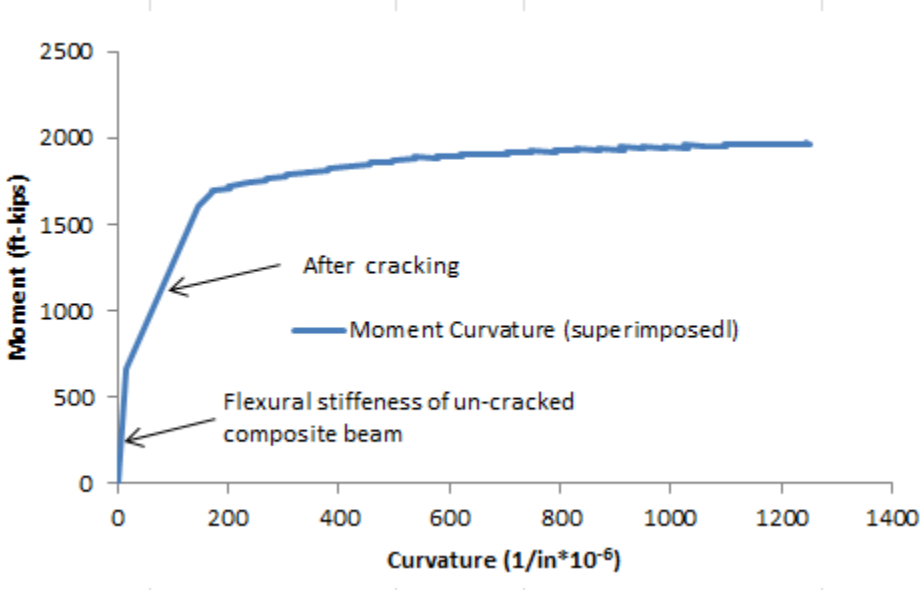

(b)

Figure 14. (a) Full moment-curvature relationship, (b) Moment-curvature relationship for superimposed loads

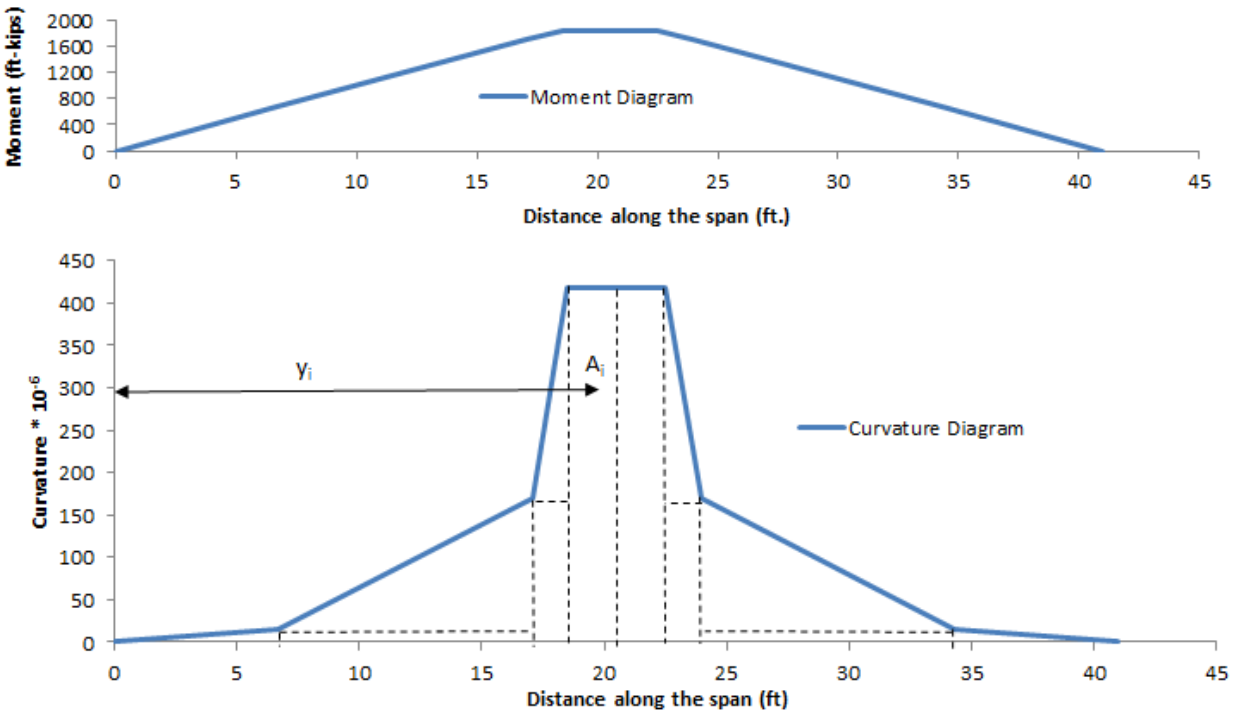

Figure 15. Moment and curvature diagram

$$\Delta_{midspan} = \sum_{i=1}^{n} A_i y_i \qquad (22)$$

RESULTS

TEST 1 – SIMULATION OF SERVICE LEVEL DESIGN MOMENT

The purpose of the first test was to load the composite beam to simulate the service level design positive moment. The actuator load required to cause this moment was estimated to be 40 kips (P_{Ms}). No cracking was observed in the precast beam during this test, which was consistent with the design requirements for a fully prestressed member. Figure 16 shows a comparison of the estimated and tested load versus mid-span deflection curves for the first test. As can be seen, the curves are almost identical which provides evidence that full composite action was maintained up until the service level moment. Also, a comparison of the load versus quarter-span deflection curves is illustrated in Figure 17. These curves are also almost identical despite the fact that one half of the span contained extended stirrups whereas the other half did not. This shows that the presence of extended stirrups is not required to ensure composite action up until the service level design positive moment. In addition, an examination of the typical load versus slip relationship at both ends of the beam, with and without extended stirrups suggests that there is no slip at either end (Figure 18 and Figure 19), and confirms the assumption for full composite action.

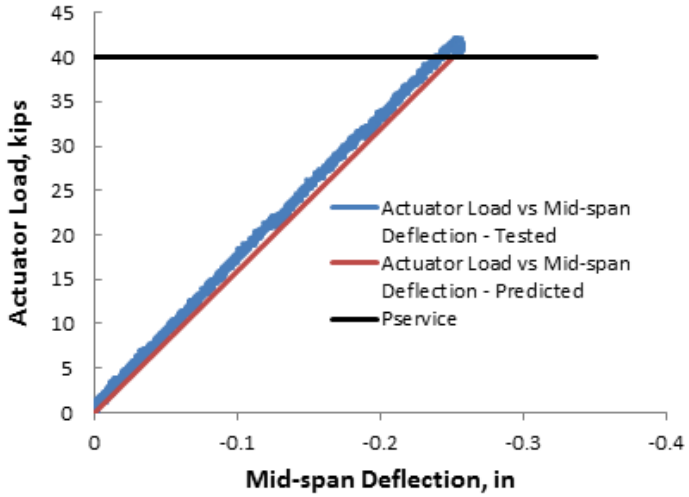

Figure 16. Comparison of predicted and experimental load vs mid-span deflection curves (up to P_{Ms})

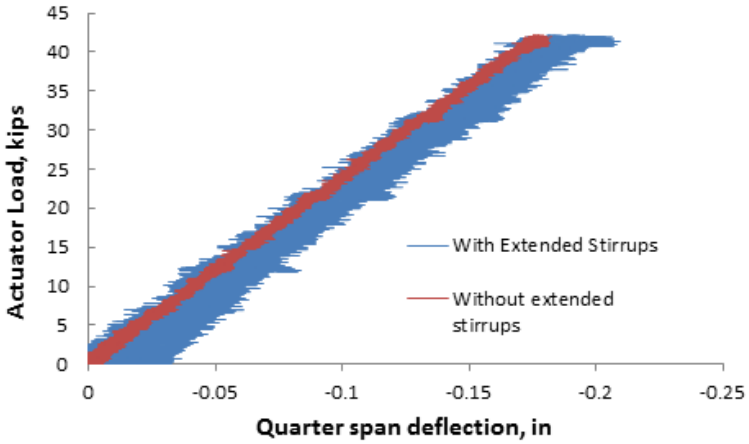

Figure 17. Comparison of load quarter span deflection curves (up to P_{Ms})

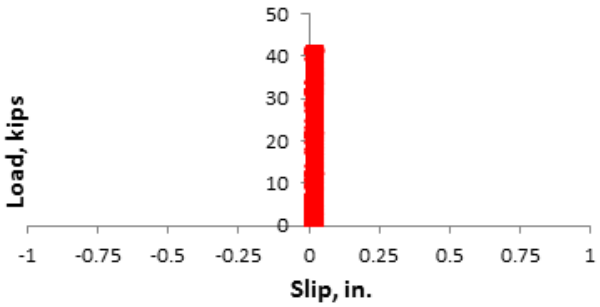

Figure 18. Typical load vs slip relationship – without extended stirrups (up to P_{Ms})

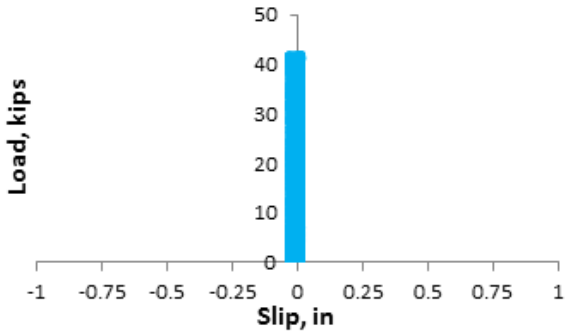

Figure 19. Typical load vs slip relationship –with extended stirrups (up to P_{Ms})

TEST 2 – SIMULATION OF STRENGTH LEVEL DESIGN SHEAR (V_u)

The purpose of the second test was to simulate strength level design vertical shear on the portion of the beam without the extended stirrups. The actuator load required to simulate this condition was estimated to be 118 kips (P_{Vu}). Figure 20 and Figure 21 reveal that there was no slip at either end of the beam under this load arrangement, which confirmed the hypothesis that the composite beam can resist the strength level design shear force without incurring any slip even with no extended stirrups. The maximum horizontal shear stress computed using Equation 1 was 99 psi. This observation leads to the conclusion that the design for horizontal shear of composite bridge systems consisting of adjacent precast inverted T-beams with tapered webs and cast-in-place topping can be confidently based on a cohesion factor equal to at least 99 psi.

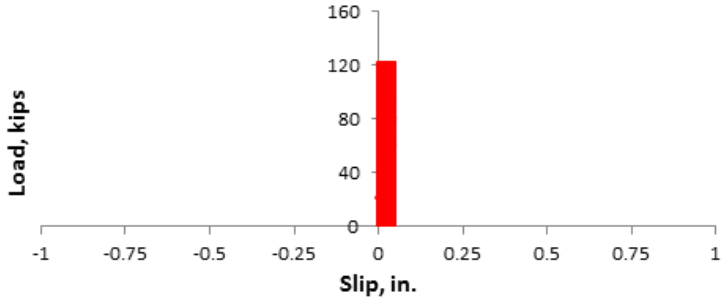

Figure 20. Typical load vs slip relationship – without extended stirrups (up to P_{Vu})

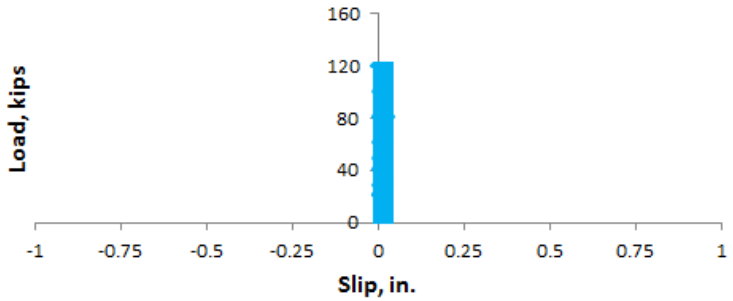

Figure 21. Typical load vs slip relationship – with extended stirrups (up to $P_{Vu)}$

TEST 3 – SIMULATION OF NOMINAL MOMENT CAPACITY (M_n)

The purpose of the third test was to simulate moments in the composite section that were equal to the strength level design positive moment and the nominal moment capacity of the composite section. The actuator load required to simulate the strength level design positive moment and nominal moment capacity was 76 kips (P_{Mu}) and 200 kips (P_{Mn}), respectively. The capacity of the actuator was 220 kips. The composite beam was loaded until the capacity of the actuator was met. Figure 22 shows a comparison between the estimated actuator load versus mid-span deflection curve to the experimentally obtained curve. It can be seen that the two curves are similar with the experimental curve exhibiting slightly higher strength and stiffness. A part of the small difference between the experimental and predicted curve can be attributed to the fact that tension stiffening was ignored in the prediction method used herein. Figure 23 shows a comparison of the actuator load versus quarter span deflection relationship. As can be seen, the two curves are identical, which suggests that the behavior of the half of the span without extended stirrups is identical to that of the other half of the span, which features extended stirrups. This observation confirms the hypothesis that the presence of extended stirrups is not required to maintain full composite action up to the development of the nominal moment capacity of the composite beam.

Figure 24 and Figure 25 show that there is no slip at either end of the composite beam, an observation that provides additional evidence about the ability of the composite beam to develop its nominal moment capacity without incurring any slip. The maximum vertical shear force at the critical section when the actuator load reached 220 kips was equal to 147 kips, which was larger than the strength level design vertical shear forces at the critical section (138 kips). Because the failure mode of the composite beam under the loading arrangement illustrated in Test 3 was of interest, the 220 kip actuator was replaced with a 400 kip actuator, and the composite beam was loaded to failure. The composite beam failed in flexure at an actuator load of 272 kips. The corresponding vertical shear force at the critical section was 173 kips including the self-weight of the composite beam. The horizontal shear stresses computed using Equation 1,2 and 3 in the previously investigated planes are provided in Table 6. The maximum computed horizontal shear stress was 124 psi in Plane 1 and was based on Equation 1. Although the composite beam at failure exhibited significant flexural cracking, the regions near the support, with the highest vertical shear did not exhibit cracking. Accordingly, the utilization of Equation 1 for these regions is valid. In addition, the horizontal shear stresses computed using Equation 3 in Planes 1 and 2 were 120 psi. As expected, horizontal shear stresses computed using Equation 4 were lower and were equal to 110 psi for Planes 1 and 2 and 95 psi for Plane 3. Because Equation 3 is provided in AASHTO as a reasonable approximation of the horizontal shear stress, these results suggest that the design for horizontal shear of adjacent precast inverted T-beams with tapered webs and cast-in-place topping can be confidently based on the following cohesion and friction factors:

$c = 120$ $\mu = 1.0$ $K_1 = 0.2$ $K_2 = 0.8$

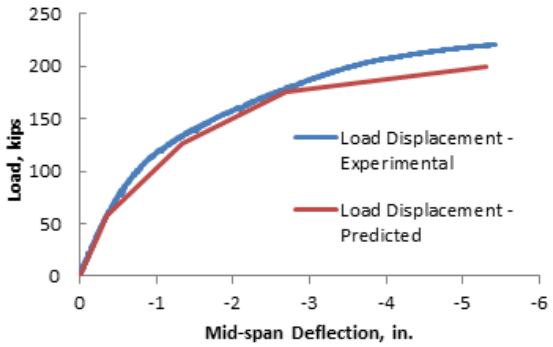

Figure 22. Comparison of predicted and experimental load vs mid-span deflection curves (Full Curve)

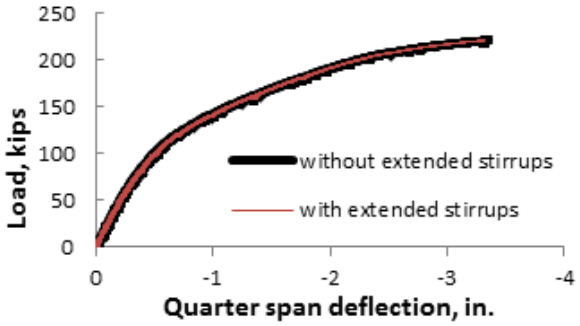

Figure 23. Comparison of load quarter span deflection curves (up to P_{Mn})

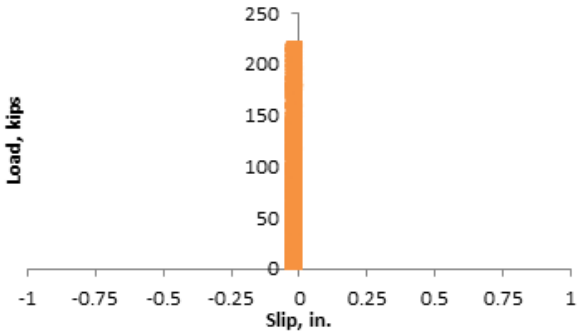

Figure 24. Typical load vs slip relationship – without extended stirrups (up to P_{Mn})

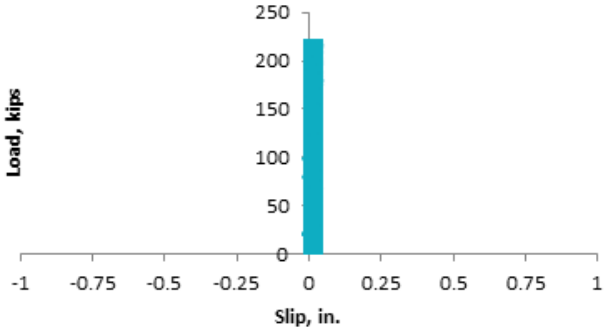

Figure 25. Typical load vs slip relationship – with extended stirrups (up to P_{Mn})

Table 6. Horizontal shear stress (based on actuator load that caused failure)

Equation	Horizontal shear stress (psi)		
	Plane 1	Plane 2	Plane 3
1	124	82	Varies
3	120	120	NA
4	110	110	95

NA = not applicable

Because of the flexural failure mode, the 120 psi horizontal shear stress representing the recommended cohesion factor does not constitute the maximum horizontal shear stress that can be developed in the composite inverted T-beam system described herein. The flexural failure of the composite beam prevented it from achieving higher horizontal shear stresses at the interfaces such as those achieved by French et al.[11] (135 psi) in their experiments.

CONCLUSIONS AND RECOMMENDATIONS

The analytical and experimental results presented in this paper lead to the following conclusions and recommendations:

- The full scale test described in this paper has demonstrated that full composite behavior is assured not only at service and strength level design loads, but also up to flexural failure in such a uniquely shaped composite system.

- The presence of extended stirrups in one half of the span did not result in any differences in behavior between the two halves of the span. Because the composite inverted T-beam bridge system with tapered webs and cast-in-place topping features a broad contact surface between the precast and cast-in-place components, adequate horizontal shear resistance along the interface to develop the nominal moment capacity of the composite section can be provided solely by the natural adhesion and friction between the two components.

- The composite bridge system described in this paper and used in the construction of the US 360 Bridge was able to develop at least a horizontal shear stress equal to 120 psi without the presence of extended stirrups. The failure mode of the composite section was a flexural failure. Because Equation 3 is provided in AASHTO as a reasonable approximation of the horizontal shear stress, these results suggest that the design for horizontal shear of adjacent precast inverted T-beams with tapered webs and cast-in-place topping can be confidently based on the following cohesion and friction factors:

  $c = 120$ $\mu = 1.0$ $K_1 = 0.2$ $K_2 = 0.8$

  Because of the flexural failure mode, the 120 psi horizontal shear stress representing the recommended cohesion factor does not constitute the maximum horizontal shear stress that can be developed in the composite inverted T-beam system described herein. The

flexural failure of the composite beam prevented it from achieving higher horizontal shear stresses at the interfaces such as those achieved by French et al.[11] (135 psi) in their experiments.

- Roughening the tapered webs and the tops of the precast flanges in the longitudinal direction while providing a transverse rake finish only at the top of the precast web appears to provide adequate horizontal shear resistance in the longitudinal direction to resist at least a horizontal shear stress of 120 psi without the presence of extended stirrups. The minimum reinforcement requirements for cases in which the horizontal shear stress is smaller than 120 psi and the precast surfaces are roughened as described above can be waived for composite bridges consisting of adjacent precast inverted T-beams with tapered webs and cast-in-place topping.

ACKNOWLEDGEMENTS

This research was sponsored by the Virginia Department of Transportation. The help and the insightful comments of Andy Zickler from the Virginia Department of Transportation and Mike Brown from Virginia Transportation Research Council are greatly appreciated. Also, the help of Mark Jones undergraduate research assistant was instrumental in the completion of the experimental investigation.

REFERENCES

1. Nilson, A. H. "Design of prestressed concrete." (1978), John Wiley & Sons.
2. Loov, R.E., Patnaik, A.K., (1994). Horizontal shear strength of composite concrete beams with a rough interface", *PCI Journal*, 39(1), 48-68.
3. Hanson, N. W. (1960), "Precast-Prestressed Concrete Bridges 2: Horizontal Shear Connections", Portland Cement Association, Research and Development Laboratories.
4. Saemann, J. C., & Washa, G. W. (1964, November), "Horizontal Shear Connections Between Precast Beams and Cast-in-Place", *ACI Journal Proceedings* (Vol. 61, No. 11). ACI.
5. 2012 AASHTO LRFD Bridge Design Specifications 6th Edition, Washington, DC
6. ACI 318-2008, Building Code Requirements for Structural Concrete and Commentary, Farmington Hills, MI
7. 2005 AASHTO LRFD Bridge Design Specifications 3rd Edition, Washington, DC
8. 1997 AASHTO Standard Specifications for Highway Bridges 16th Edition, American Association of State Highway Officials, Washington, DC
9. Menkulasi, F., Mercer, M., Wollmann, C. L .R, Cousins, T., "Accelerating Bridge Construction Using The Precast Inverted T-Beam Concept", *PCI 2012 Convention and National Bridge Conference,* September 29 -October 02, 2012.
10. Menkulasi, F., Wollmann, C.L.R., Cousins, T., "Investigation of Time Dependent Effects on Composite Bridges with Precast Inverted T-Beams", *PCI 2013 Convention and National Bridge Conference*, September 21-24, 2013.

11. French. C.W., Shield, C.K., Klasesus, D. Smith, M., Eriksson, W., Ma, J.Z., Zhu, P., Lewis, S., Chapman, C.E. - "Cast-in-Place Concrete Connections for Precast Deck Systems" – *NCHRP Web-Only Document 173* – January 2011 – National Cooperative Highway Research Program – Transportation Research Board of the National Academies
12. Kent, D.C., and Park, R. (1971). "Flexural members with confined concrete." Journal of the Structural Division, Proc. of the American Society of Civil Engineers, 97(ST7), 1969-1990.
13. Kovach J.D., Naito, C., Horizontal Shear Capacity of Composite Concrete Beams without Ties, ATLSS Report No. 08-05, PCI / PITA Research Project, Bethlehem, PA